A Reduced Swift-Hohenberg Style Model for Vegetation Patterns in Drylands

Amanda Vanegas Ledesma
Mentors: Alasdair Hastewell and Davis Evans
Project Suggested by: Profs. John Bush and Jörn Dunkel

August 5, 2021

Abstract

One in three people worldwide live in drylands, which are particularly vulnerable to desertification. In these ecosystems, where natural resources are limited, vegetation survives by organizing itself into patterns. The ecological factors governing these patterns were captured by Zelnik and others in a reaction-diffusion model consisting of two coupled equations for groundwater and biomass. In this paper, we leverage the strong water-biomass relation suggested by our simulations to derive a groundwater equation in terms of biomass and its spatial derivatives. Through this procedure we reduce Zelnik's model to a single Swift-Hohenberg style biomass equation. Our model differs from the classical Swift-Hohenberg models in that nonlinear terms multiply second and higher spatial derivatives of biomass. This feature reflects that vegetation regulates its own water induced growth. The model presented shares the pattern forming properties of Swift-Hohenberg models, making it mathematically tractable while conserving clear ecological meaning. Hence, our biomass equation allows for the extensive study of drylands' resilience to changing climate conditions.

Figure 1: On the left, cloud streets over the Labrador sea, picture from NASA Earth Observatory. On the right, zebras' stripes create an optical illusion that help them run from predators. (Image from the BBC)

1 Introduction and Background

Far from being random and disorganized, the natural world exhibits a complex structure that outshines the some of the best architectural master pieces. The most striking examples include cloud streets, animal coatings, and patterns in drylands vegetation.

More importantly, for a wide range of natural systems, patterns are not only aesthetically appealing but also crucial for their existence. In the atmosphere, cloud streets are significant for the vertical transport of momentum, heat, moisture, and air pollutants [1]. For animals, patterned coating is essential for survival: zebras' stripes help them camouflage and cheetahs' spots enable them to hunt [2]. In drylands vegetation, self-organization into patterns allows for a more efficient use of the limited natural resources, such as water and soil nutrients [3].

In the past, vegetation irregularities were attributed to topography and soil heterogeneities, it was not until the first aerial photographs were available that regular vegetation patterns such as gaps, spots, stripes, and even intricate labyrinths were observed [4].

These patterns are ubiquitous in drylands, areas that face great water scarcity and cover around 40% of earth's land surface [5]. These areas have adapted to climatic variability and water stress, but they are still highly vulnerable to climate change and damaging human activities such as deforestation and unsustainable agricultural practices [3]. The extreme environmental conditions faced by drylands makes them particularly at risk of desertification, the process of change in soil properties, vegetation, and climate that

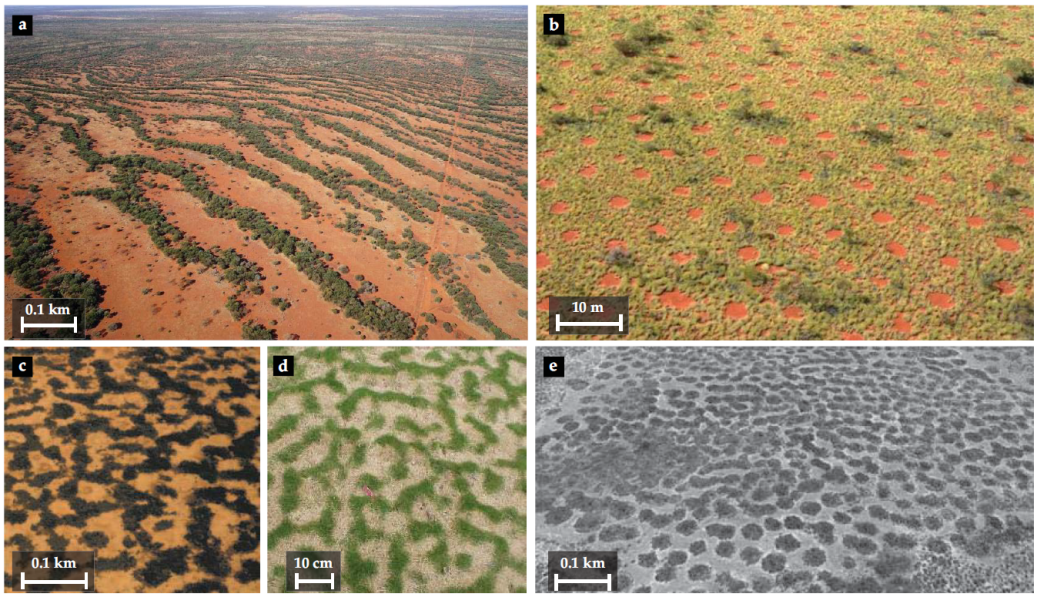

Figure 2: Different patterns observed in dryland vegetation. **(a)** Banded vegetation on a sloped terrain, Australia. **(b)** Gap pattern, Australia. **(c)** Labyrinthine pattern, in Niger. **(d)** Labyrinthine grass pattern, in Israel. **(e)** Spot pattern, in Zambia. Image from [4]

results in the ecosystem permanently losing its capability to sustain life [5].

Given the current climate conditions, ecosystems are threatened more than ever before. One of the main factors that influences vegetation cover is precipitation, which will be immediately affected by changes in climate dynamics[6]. Drylands are disproportionately impacted: over the last 100 years, the largest warming was observed over drylands [7], and accounted for more than half of the global warming.

When water availability is limited, vegetation patterns become critical for ecosystems' survival. A decrease in precipitation might cause an uniform vegetation cover to cease being stable. Without patterns, this vegetation cover would be substituted by bare soil, causing the landscape to essentially become a desert. Therefore, by creating patterns vegetation is able to make a better use of the available resources and increase its resilience to desertification[8].

In the presence of high temperatures and reduced precipitation, it becomes increasingly relevant to understand the factors that lead to ecosystem

collapse and how it can be prevented. The growing recognition of these patterns as a fundamental phenomenon has lead to the emergence of a research field that connects ecology, non-linear physics, and applied mathematics.

The stochastic nature of the numerous ecological factors that govern vegetation constitutes one of the main challenges to obtain models that are mathematically tractable and conserve a clear ecological meaning [3]. Previous work have focused on developing a phenomenological model that capture the complex water-vegetation dynamics of a water limited ecosystems. The proposed model by Zelnik *et al.* [9], embodied into a reaction-diffusion framework, describes a large amount of ecological effects and successfully reproduce patterns observed in drylands. However, the large number of parameters included in the model complicates its mathematical study. On the other hand, there are already well studied models which are known to create patterns. In particular, the Swift-Hohenberg equation has been extensively studied [10] and is known to capture patterns similar to those present in vegetation. Nonetheless, as it is not meant to specifically describe vegetation, its connection with ecology is unclear. Through this work, we start from Zelnik *et al.* [9] model, which consists on two coupled equations describing the evolution of water and biomass, and derive a Swift-Hohenberg style equation that allows for mathematical tractability while conserving clear ecological meaning.

The present work is structured as follows. Section 1.1 introduces reaction-diffusion equations and the Swift-Hohenberg model, and we describe their pattern formation properties by doing a linear stability analysis. Then in section 2 we describe current vegetation pattern formation models and show the range of patterns we can achieve through simulating Zelnik *et al.* model. Next, in section 3 we derive an equation for groundwater in terms of biomass and its spatial derivatives. Finally, in section 4 we use the derived groundwater equation to propose a modified Swift-Hohenberg model that describes vegetation pattern formation.

1.1 Mathematical Modeling of Pattern Formation

Some of the first insightful ideas about mathematical modeling of pattern formation were presented by Alan Turing in 1952. In his seminal paper "The chemical basis of morphogenesis" [11], he proposed that diffusion in a chemical reaction can actually destabilize a uniform system driving it to spatially periodic patterns. For this to occur, the system needs to consists of at least

two interacting chemicals with very different diffusion rates. Typically, the diffusion rates differ by a factor of 10 or more [12]. In such a reaction-diffusion system, there is typically a local activator and a long-range inhibitor. Given a small perturbation of an equilibrium stat at an specific spot, the activator will locally enhance the growth of both species. Far from the initial growth spot, the inhibitor stops the activator's growth and its own. Thus, the interaction of both substances breaks the spatial symmetry of the system, creating patterns.

These following classical models give a mathematical description of this effect and the conditions necessary for pattern formation.

1.1.1 Reaction-Diffusion Equations

The general form of the reaction-diffusion model for two chemical concentration fields, $u = u(t, x)$ and $v = v(t, x)$ studied by Turing has the form:

$$\partial_t u = f_1(u, v) + D_1 \partial_x^2 u, \tag{1a}$$
$$\partial_t v = f_2(u, v) + D_2 \partial_x^2 v, \tag{1b}$$

where ∂_t indicates the time derivative and ∂_x indicates the spatial derivative. Defining the vector $\mathbf{u} = (u, v)$, one can rewrite Eqs. (1) in vector form:

$$\partial_t \mathbf{u} = \mathbf{f}(\mathbf{u}) + \mathbf{D}\partial_x^2 \mathbf{u}, \tag{2}$$

where $\mathbf{D}$ is the $2D$ matrix:

$$\begin{pmatrix} D_1 & 0 \\ 0 & D_2 \end{pmatrix} \tag{3}$$

To study the conditions under which a reaction-diffusion system like the one above create patterns we perform a linear stability analysis, following Cross and Greenside [12]. We start by finding a uniform steady state, by setting all the partial derivatives to zero and solving

$$\mathbf{f}(\mathbf{u}_\star) = 0. \tag{4}$$

In the absence of diffusion, the fixed point $\mathbf{u}_\star = (u_\star, v_\star)$ is linearly stable if

$$\mathbf{Tr}(\mathbf{J}) < 0, \text{ and} \tag{5a}$$
$$\mathbf{Det}(\mathbf{J}) > 0. \tag{5b}$$

Where J is the Jacobian matrix evaluated at the steady state $\mathbf{u}_\star$. Consider a small perturbation $\mathbf{u}_p$ around the steady state $\mathbf{u}_\star$. It can be shown that an arbitrary infinitesimal perturbation will evolve according to [12]:

$$\partial_t \mathbf{u}_p = \mathbf{J}\mathbf{u}_p + \mathbf{D}\partial_x^2 \mathbf{u}_p \mathbf{u}_p \mathbf{u}_p \mathbf{u}_p, \tag{6}$$

Now, assuming a plane wave form for the perturbation:

$$\mathbf{u}_p = \mathbf{u}_q e^{\sigma_q t} e^{iqx}, \tag{7}$$

where $\mathbf{u}_q$ is a constant vector, σ_q is the growth rate of the perturbation, and q is the wave vector defined as $2\pi/\mathbf{L}$. Where $\mathbf{L} = (Lx, Ly)$ gives the characteristic wavelength of the perturbation in the x and y directions. The base state $\mathbf{u}_\star$ of the system of Eqs. (1) remain stable if and only if σ_q is negative for all wave numbers q. By linearizing around the base state $\mathbf{u}_\star$ it can be shown that the growth rate of a mode with wave number q, σ_q, is a solution to the eigenvalue problem

$$(\mathbf{J} \text{ - } \mathbf{D}q^2)\mathbf{u}_q = \sigma_q \mathbf{u}_q, \tag{8}$$

Assuming that $\mathbf{u}_\star$ satisfies Eq. (5), it can be shown that diffusion destabilizes the system if and only if

$$\mathbf{Det}(\mathbf{J} - q^2\mathbf{D}) > 0. \tag{9}$$

If these conditions hold, so that Eqs. (1) have a base state $\mathbf{u}_\star$ which is stable without diffusion and becomes unstable with diffusion, the system exhibits a **Turing instability**. This type of instability is well known for generating patterns and it is the base of the pattern formation properties of the vegetation patterns presented in this paper.

1.1.2 Swift-Hohenberg Model

To achieve instabilities that lead to pattern formation in a single species model, it is necessary to include not only diffusion but also a 4th order spatial derivative into the evolution equation. In this sense, the Swift-Hohenberg

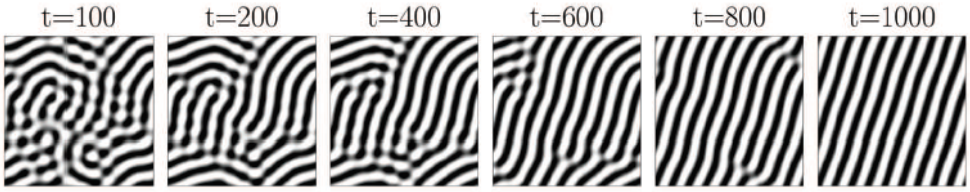

Figure 3: Simulation of an SH model showing the relaxation from disordered stripes pattern to an ordered stationary striped pattern. Parameters: $N(u) = -u^3$, $r = 0.1$. From [13].

(SH) model is the simplest PDE model that captures an instability of a stationary uniform state to periodic patterns [13]. It can be written as:

$$\partial_t u = \lambda u - (1 + \nabla^2)^2 u + N(u), \tag{10}$$

where $N(u)$ is some smooth non-linearity and r acts as a bifurcation parameter. It was originally derived to model thermal convection in a shallow liquid layer [14] but has become a canonical model for pattern formation studies in general [12]. Fig. 3 shows a simulation of the SH model, revealing the creation of an ordered stripe pattern [13].

To understand the pattern formation properties of the SH equation, we follow a linear stability analysis, as suggested by Cross and Greenside [12], of Eq. (10) with λ as the bifurcation parameter. Similarly to the linear stability analysis of the reaction-diffusion model, they show that by considering a perturbation $u_p = u_q e^{\sigma_q t} e^{iqx}$ around a stationary solution u_b, one can find how the growth rate σ_q of a Fourier mode of wave number q depends on the system parameters.

As an example of the growth rate near an instability of the SH model, Cross and Greenside find σ_q for Eq. (10) with $N(u) = -u^3$. Fig. 4 shows their results. In the Figure, the growth rate σ_q is plotted versus the wave number q for the uniform base state $\mathbf{u}_b = 0$. It can be observed that for values of the parameter λ above a critical value of $\lambda_c = 0$, perturbations of the base state will grow, generating patterns of characteristic length scale $2\pi/q_c$, where q_c is the critical wave number at which $\sigma = 0$.

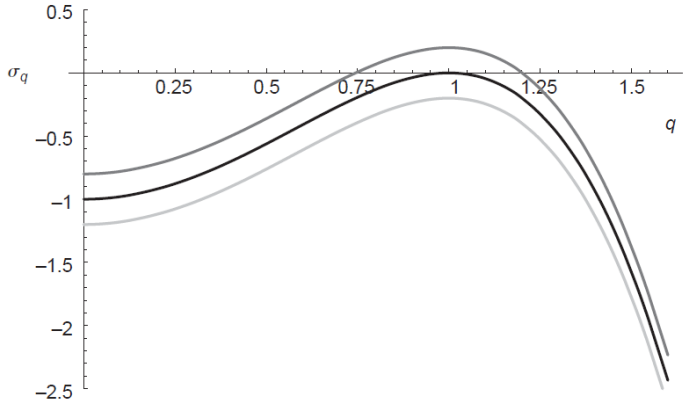

Figure 4: Growth rate σ_q, versus the wave number q for the uniform base state $\mathbf{u}_b = 0$ of the one-dimensional Swift–Hohenberg equation Eq. (10) with $N(u) = -u^3$. The curves shown correspond, respectively to $\lambda = -0.2$ (light gray), $\lambda_c = 0$ (black), and $\lambda = 0.2$ (dark gray). These correspond to a stable, marginally unstable, and unstable base state. For values slightly above λ_c a narrowband of Fourier modes centered on the critical wave number can grow, resulting in the appearance of a pattern [12]

1.1.3 Vegetation Patterns

Mathematical models of vegetation patterns are based on the interaction between water and biomass. Because water diffuses faster than plants spread seeds and reproduce, we can think about vegetation patterns growth as an activator-inhibitor system. Consider a vegetation spot, the local growth of vegetation induced by water constitutes the short-range activator, while the lack of water far from the vegetation spot combined with the long time plants would take to grow, constitutes the long-range inhibitor. Zelnik's model, which we will elaborate on in the following section in the paper, constitutes a two-species (plant biomass and groundwater) reaction-diffusion model. Inspired by the simple form of the SH model, in this work we reduce Zelnik's model to a single equation model that describes the evolution of the biomass and includes higher spatial derivatives thereof.

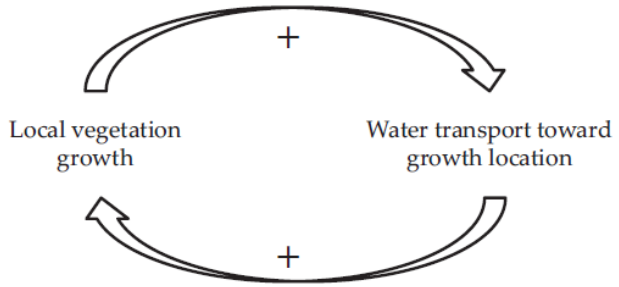

Figure 5: A positive feedback loop drives vegetation patterns in water-limited ecosystems. Water accelerates vegetation growth, while denser patches of vegetation induce water transport towards themselves. From [4].

2 Mathematical Modeling of Vegetation Patterns

In water-limited ecosystems, a positive feedback loop between vegetation growth and water availability arises [4]. Consider a terrain of uniform vegetation with a slightly denser vegetated patch. Figure 5 shows a schematic of this loop: the localized vegetation induces water transport towards the denser patch (lower arrow in the loop), while the increase of water availability will promote biomass growth, making the vegetated patch even denser (upper arrow in the loop).

While it is intuitive that water near plants induces growth, it is less obvious why the presence of plants induces water transport, so implying the positive feedback. Three key mechanisms that promote water transport towards denser vegetated areas are depicted in Fig. 6: overland flow, lateral roots, and soil-water diffusion [4].

Areas depleted from vegetation receive direct sunlight, creating ideal conditions for bacteria to grow and causing the creation of a physical or biological crust that limits the infiltration of water. In vegetated areas infiltration is enhanced by not only the lack of this crust but also the pressure of roots penetrating the soil, which results in an overland flow of water towards densely vegetated patches, Fig. 6**a**. Moreover, when roots extend laterally, these deplete the surrounding soil from water, enhancing the difference in biomass between a spot of vegetation and its surroundings, Fig. 6**b**. Finally, in systems with laterally confined roots, strong water uptake by deeper roots

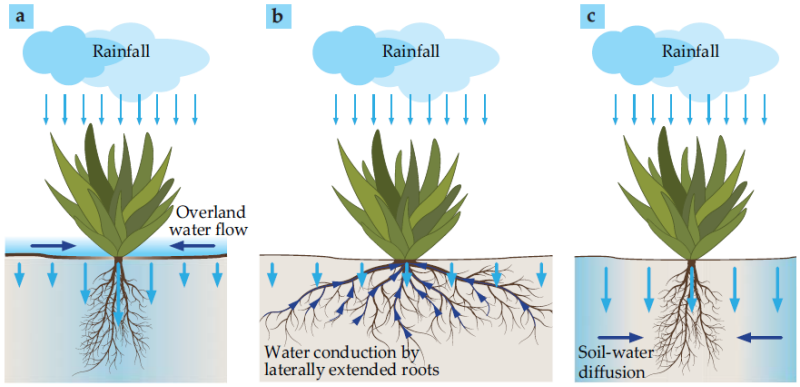

Figure 6: Three forms of water transport promote flow towards regions of denser vegetation. **(a)** Overland water flow takes water towards vegetated areas, which have higher infiltration rate than bare soil. **(b)** Laterally extended roots deplete areas surrounding vegetation patches from water. **(c)** Soil water diffusion brings water from non-vegetated areas to water-poor soil vegetated areas. From [4].

depletes the water content of the soil relatively to its surroundings, creating a gradient in groundwater that causes water to diffuse towards areas of accelerated vegetation growth, Fig. 6**c**.

These three feedback mechanisms were described by Gilad *et al.* 2004 [15]. They proposed a three equations model to describe the evolution of biomass (B [kg/m^2]), groundwater (W [kg/m^2]) and a thin height of water above the surface (H [m]). In its dimensional form this model is:

$$\partial_t B = G_b \lambda B(1 - B/K) - MB + D_B \nabla^2 b, \tag{11a}$$
$$\partial_t W = IH - N(1 - RB)W - \lambda G_w W + D_w \nabla^2 W, \tag{11b}$$
$$\partial_t H = P - IH + D_H \nabla^2 (H^2) + 2\nabla H \cdot \nabla \zeta + 2H\nabla^2 \zeta, \tag{11c}$$

In the biomass equation, Eq. (11a), $B(1 - B/K)$ describes to the logistic growth of the biomass, where $B = K$ is the maximum standing biomass. Logistic growth indicates that the biomass growth is proportional to the existing biomass and the amount of available resources [16]. This growth is modulated by the water availability given by G_b, MB corresponds to biomass mortality, and $D_b \nabla^2 B$ to diffusion of seeds. In the water equation, Eq. (11b),

I is the infiltration rate of water into the soil, $N(1-RB)W$ accounts for the evaporation of water, reduced by a factor of (1 - RB) due to shading from the biomass, where N is the evaporation rate and R is a shading factor between 0 and 1. The consumption of water by vegetation is given by $G_w W$, and $D_w \nabla^2 W$ is the diffusion of water. The equation for H has been derived from groundwater theory, P corresponds to precipitation, and ζ gives the topography.

The infiltration rate depends on the biomass and it is given by:

$$I = AH\frac{B+QF}{B+Q}, \tag{12}$$

where A, Q and F are constants that quantify the infiltration rate of the soil. Owing to to the spatial extent of the underground roots, water uptake is non-local with respect to the above ground biomass. Their non-local relation is approximated by Gilad *et al.* through a Gaussian Kernel:

$$G_b = \Lambda \int_\Omega d\mathbf{X'},\, G(\mathbf{X}, \mathbf{X'}, T) W(\mathbf{X'}, T), \tag{13a}$$

$$G_w = \Gamma \int_\Omega d\mathbf{X'}\, G(\mathbf{X}, \mathbf{X'}, T) B(\mathbf{X'}, T) \tag{13b}$$

$$G(\mathbf{X}, \mathbf{X'}, T) = \frac{1}{2\pi S_0^2} \exp\left[-\frac{|\mathbf{X}-\mathbf{X'}|^2}{2[S_0(1+EB(\mathbf{X},T))]^2} \right], \tag{13c}$$

where E is the root-to-shoot ratio, which is the ratio of the below-ground plant (root) to the above-ground plant (shoot), and S_0 represents the lateral extend of the roots. Although this model has clear ecological significance, the integral terms make it non-local and therefore its mathematical analysis challenging. In the following, we introduce a simplified version of the model that was presented by Zelnik *et al* in [9], who reduced the three non-local PDEs to two PDEs with only local terms.

By only considering a flat terrain ($\zeta = 0$), the equation for $\partial_t H$ reduces to $P - I$. Furthermore, if the landscape is highly porous, the infiltration rate can be assumed to be high everywhere, independently of vegetation. Therefore, $P \simeq I$, which completely eliminates H as a state variable.

If the lateral extent of the roots is small compared to their vertical length scale, then the biomass growth only depends on the soil water directly beneath it. Thus the non-local terms, G_b and G_w can be approximated as $(1+EB)^2 W$ and $(1+EB)^2 B$ respectively.

To non-dimensonalize the equations we re-scale the state variables B, W and the space and time derivatives as

$$b = \frac{B}{K}, \qquad w = \frac{W\Lambda}{K\Gamma}, \qquad t = MT, \qquad x = X\sqrt{M/D_b}, \tag{14}$$

the simplified model can then be written, in its non-dimensional form as [9]:

$$\partial_t b = \lambda b w(1-b)(1+\eta b)^2 - b + \nabla^2 b, \tag{15a}$$
$$\partial_t w = p - \nu w(1-\rho b) - \lambda b w(1+\eta b)^2 + \delta_w \nabla^2 w. \tag{15b}$$

The meaning of the parameters used in the models by Gilad *et al.* and Zelnik *et al.* described above, their typical values and non-dimensionalization can be found in Tables 1 and 2.

Parameters	Meaning	Dimensions
B	Above Ground Biomass	$\mathrm{kg/m^2}$
W	Soil Water	$\mathrm{kg/m^2}$
Λ	Biomass Growth Rate	$(\mathrm{kg/m^2})/\mathrm{y}$
K	Maximal Standing Biomass	$\mathrm{kg/m^2}$
E	Root-Shoot Ratio	$\mathrm{m^2/kg}$
D_B	Seed Dispersal	$\mathrm{m^2/y}$
M	Mortality rate	$1/\mathrm{y}$
P	Precipitation rate	$\mathrm{mm/y}$
N	Evaporation rate	$1/\mathrm{y}$
R	Reduction of evaporation due to shading	1
Γ	Water uptake coefficient	$(\mathrm{kg/m^2})/\mathrm{y}$
D_W	Soil-Water diffusivity	$\mathrm{m^2/y}$

Table 1: Dimensional Parameters used in the models by Gilad *et al.* and Zelnik *et al.*, Eqs. (11).

The patterns obtained from simulating the model with the typical parameters values in Table 2 are shown in Fig. 7. We can observe how a variety of patterns, including gaps, spots, labyrinths and stripes can be obtained through this model, corresponding to the patterns commonly seen in nature, Fig. 2.

Parameters	Typical Values for the Zelnik. et al Model
$\lambda = {}^{K\Gamma}/_{M}$	0.45
$\eta = EK$	2.8
$p = {}^{\Lambda P}/_{K\Gamma M}$	0.9 - 2.7
$\nu = {}^{N}/_{M}$	1.42
$\rho = R$	0.7
$\delta_w = {}^{D_w}/_{D_B}$	125

Table 2: Non-Dimensional Parameters in Eqs. (15).

To understand the pattern forming properties of the Zelnik model we perform a linear stability analysis analogous to that of the reaction-diffusion equations presented in section 1.1.1. To put our results in ecological context, we explain the following analysis in terms of the dimensional precipitation P, whose relation with the non-dimensional parameter p in Eq. (15) can be found in Table 2. The homogeneous steady states are found by setting the time and space derivatives of the model to zero and solving:

$$f_1(b, w) = \lambda bw(1 - b)(1 + \eta b)^2 - b = 0, \tag{16a}$$
$$f_2(b, w) = p - \nu w(1 - \rho b) - \lambda bw(1 + \eta b)^2 = 0. \tag{16b}$$

This system has three physical solutions, one bare soil state given by $(b, w) = (0, {}^{p}/_{\nu})$, and two uniform non-zero steady states, (b_1, w_1) and (b_2, w_2). The trace and determinant of the Jacobian matrix of f_1 and f_2 allow us to calculate the linear stability of these three base states by applying the conditions given by Eqs. 5. Fig. 8 shows the linear stability of these equilibria in the absence of diffusion: the bare soil is always stable for the precipitation (P) values studied, (b_1, w_1) is unstable up to $P \sim 83$ and stable otherwise, and (b_2, w_2) is unstable for all the values of P considered.

We now consider a perturbation around the base state (b_1, w_1) of the form $(b_p, w_p) = (b_q, w_q)e^{\sigma t}e^{iqx}$, where b_q and w_q are constants. Subsequently, we find the precipitation values for which Eq. (6) holds for some wave number q. This analysis indicates that for precipitation values less than $P_c = 91$ mm/y, (b_1, w_1) is unstable to small perturbations. Consequently, between for $83 < P < 91$ (b_1, w_1) is destabilized by diffusion. This shows that the model given by Eqs. (15) presents a Turing instability. Near this instability the model will reproduce patterns.

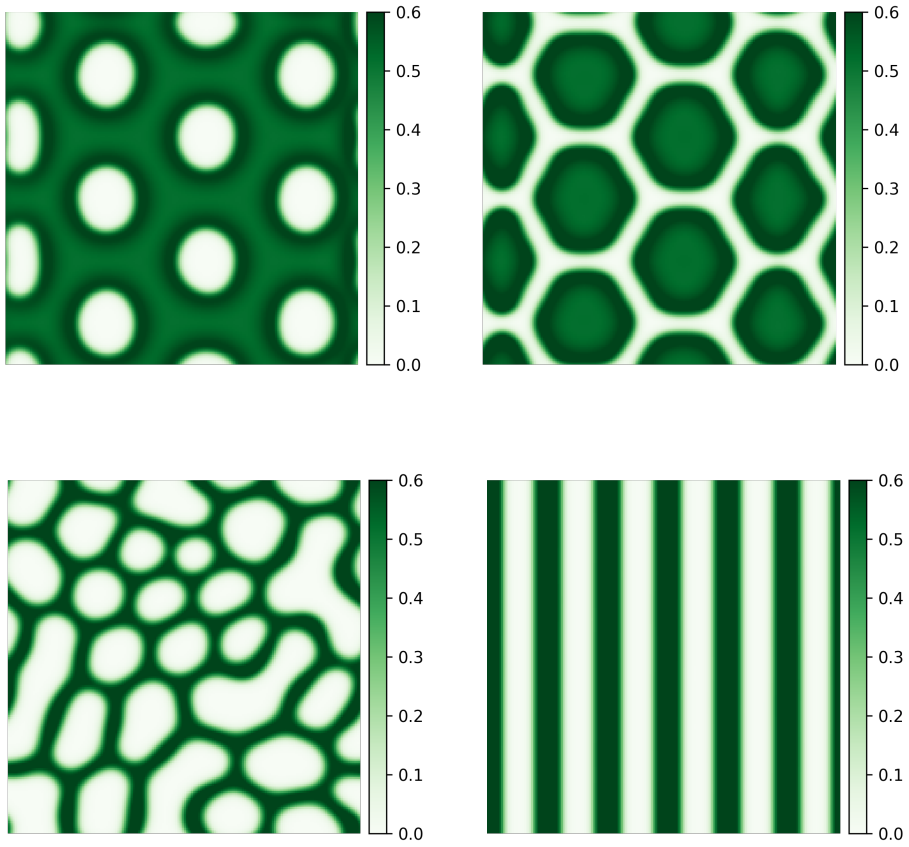

Figure 7: Patterns obtained from simulating the Zelnik's model, given by Eqs. (15). Dark green indicates vegetation, and white corresponds to bare soil. On the top row, bare soil gaps on uniform vegetation (left) and vegetation spots in bare soil (right) are shown. These hexagonal patterns have been observed in natural systems [17]. On the lower row we observe a labyrinth pattern (left) and a striped pattern (right). The striped patterns are commonly found in hills [18].

It is important to notice that the $(1 + \eta b)^2$ term in Eq. (15) is crucial for the pattern formation properties of the model. Mathematically, if we set $\eta = 0$ the only homogeneous steady state of Eq. (15) along the precipitation parameters studied is the bare soil. Therefore, a model with $\eta = 0$ does not

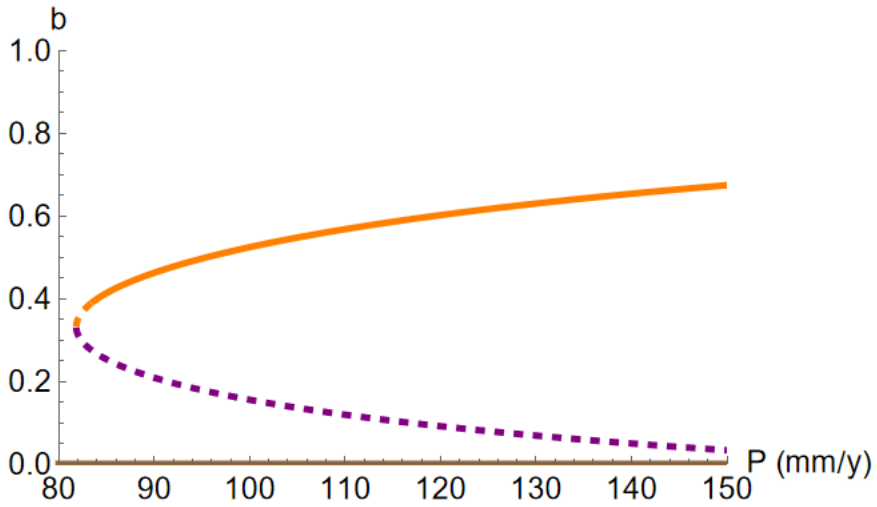

Figure 8: Bifurcation diagram of the steady states of Zelnik's model (Eqs. (15)), showing the non-dimensional biomass, b, vs. the precipitation rate, P, in dimensions of mm/y. The steady states include the bare soil (brown) and the two uniform states (b_1, w_1)(purple) and (b_2, w_2) (orange). Dashed lines indicate linearly unstable states, and full lines indicate linearly stable states. The bi-stability of two stable states is a characteristic of pattern formation.

have bi-stability of steady states nor presents a Turing instability, both of which are required for the onset of an instability that leads to patterns.

Physically, η corresponds to the root-to-shoot ratio. Therefore, $\eta \to 0$ corresponds to when the roots of the plant are insignificantly small compared to the above-ground plant. Recall that in the previous section we discussed the feedback mechanisms responsible for pattern formation: overland water flow, laterally extended roots, and groundwater diffusion. Zelnik's model, Eqs. (15), assumes that the infiltration rate is independent of biomass and roots are laterally constrained, hence the dominant water transport mechanism in the terrains studied will be the enhanced soil-water diffusion towards densely vegetated areas. This mechanism depends on the roots of the plants being deep enough to deplete the soil beneath the plant from water and create a gradient. Thus, setting η to zero would imply that there cannot be soil-water diffusion, and therefore we do not have a water-vegetation feedback mechanism to promote pattern formation in this case.

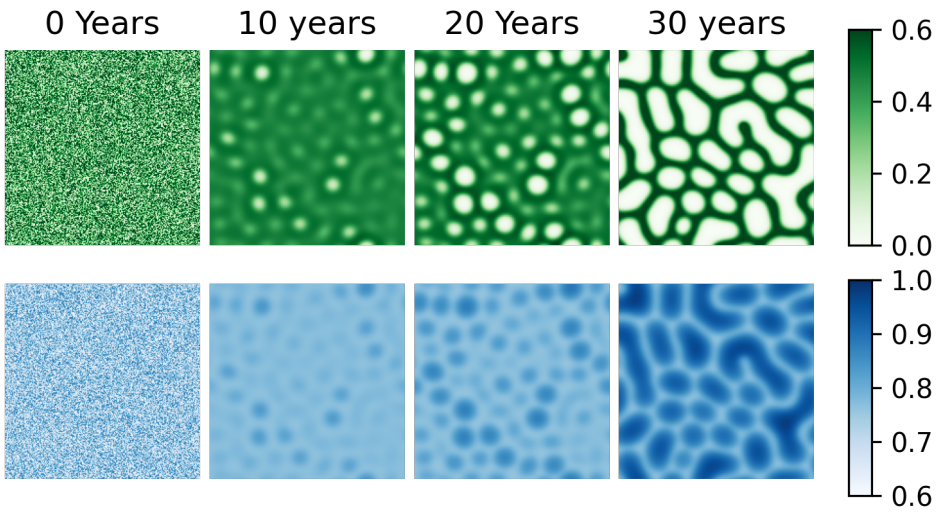

Figure 9: Biomass (top) and water (bottom) fields obtained from simulating Eqs. (15) for 30yrs, initiating from random noise. It can be observed how the spatial distribution of water and biomass are closely related throughout the evolution of the pattern, practically mirroring each other.

3 An equation for groundwater in terms of biomass

The water-vegetation feedback mechanisms described in the previous section indicate that the availability of groundwater is closely related to the presence of a vegetation cover. When the soil is assumed to have uniform infiltration, groundwater is expected to be concentrated in areas depleted of vegetation, where water from precipitation infiltrated but it has not been consumed by the plants. Fig. 9 shows the result of simulating Eqs. (15) from uniform noise intial conditions to a steady state. Here, it can be observed how the spatial distribution of vegetation cover and groundwater are closely related.

This relation suggests that groundwater can be modeled as a function of biomass: $w = w(b)$. To derive this equation, we proceed by solving for w in terms of b in the original two-equation Zelnik's model given by Eqs. (15).

Groundwater moves on time scales much faster than the biomass. Evaporation, soil infiltration and diffusion through porous media have a time scale

of hours, while biomass growth occurs over years or even decades. Therefore, it can be assumed that w reaches an equilibrium much faster than b. Considering this simple limit, the time derivative of w is set to zero, obtaining a local in time but non-local in space relationship between b and w:

$$(\nabla^2 - k^2)w(\mathbf{x}) = -\epsilon^2 p, \tag{17}$$

where

$$\begin{aligned} k^2 &= \frac{1}{\delta_w}[\nu(1-\rho b) + \lambda b w(1+\eta b)^2], \\ &= \frac{1}{\delta}[\nu - b(\nu\rho - \lambda) + b^2(2\eta\lambda) + b^3(\eta^2\lambda)]. \end{aligned}$$

For the sake of mathematical tractability, we temporarily assume that that k is constant, allowing for the change of variables $\tilde{\boldsymbol{x}} = \mathbf{x}/k$. Substituting into Eq. (17):

$$(\tilde{\nabla}^2 - 1)w(\tilde{\boldsymbol{x}}) = -\frac{1}{\delta_w}\frac{p}{k^2}. \tag{18}$$

In the remaining derivation k is no longer constant, and b is again allowed to vary in time and space. Expanding $1/(\delta_w k^2)$ around $b = 0$ yields:

$$(\nabla^2 - 1)w = -(p/\nu + \phi_1 b + \phi_2 b^2 + \cdots), \tag{19}$$

where the tildes were dropped for notational simplicity, and the ϕ_i's are constant coefficients which depend on the environmental parameters ν, λ, ρ, etc. The solution for $w(\mathbf{x})$ may be readily written in terms of the Green's function for the $(\nabla^2 - 1)$ operator. Given this function, $G(\mathbf{x} - \mathbf{x}')$, we can solve for $w(x)$:

$$w(\mathbf{x}) = -\int d\mathbf{x}'\, G(\mathbf{x} - \mathbf{x}')\left(\frac{p}{\nu} + \phi_1 b\right). \tag{20}$$

In 2D the Green's function for $(\nabla^2 - 1)$ is

$$G(\mathbf{x} \text{ - } \mathbf{x}') = -\frac{1}{2\pi}K_0(|\mathbf{x} \text{ - } \mathbf{x}'|). \tag{21}$$

Now, we have a non-local equation for groundwater. To obtain an equation for groundwater that only depends on biomass, we approximate the integral

in the previous equation in terms of spatial derivatives of biomass. To achieve this we are going to use the Fourier transform of this Green's function. To derive this, we first define a Fourier convention:

$$\begin{aligned} f(\mathbf{x}) &= \int d\boldsymbol{\omega}\, \hat{f}(\boldsymbol{\omega}) e^{2\pi i \mathbf{x}\cdot\boldsymbol{\omega}}, \\ \hat{f}(\boldsymbol{\omega}) &= \int d\mathbf{x}\, f(\mathbf{x}) e^{-2\pi i \mathbf{x}\cdot\boldsymbol{\omega}}. \end{aligned} \tag{22}$$

Subsequently, consider a function $G(\mathbf{x}-\mathbf{x}')$ such that:

$$(\nabla^2 - 1)G(\mathbf{x}-\mathbf{x}') = \delta(\mathbf{x}-\mathbf{x}'). \tag{23}$$

Transforming to Fourier space and multiplying by $e^{2\pi i \mathbf{x}'\cdot\boldsymbol{\omega}'}$:

$$\delta(\mathbf{x}-\mathbf{x}')e^{2\pi i \mathbf{x}'\cdot\boldsymbol{\omega}'} = -\int d\boldsymbol{\omega}\, (4\pi^2|\boldsymbol{\omega}|^2 + 1)\hat{G}(\boldsymbol{\omega}) e^{2\pi i \mathbf{x}\cdot\boldsymbol{\omega}} e^{-2\pi i \mathbf{x}\cdot(\boldsymbol{\omega}-\boldsymbol{\omega}')}. \tag{24}$$

Integrating with respect to $\mathbf{x}'$ and applying properties of the delta function, we obtain:

$$e^{2\pi i \mathbf{x}\cdot\boldsymbol{\omega}'} = -\int d\boldsymbol{\omega}\, (4\pi^2|\boldsymbol{\omega}|^2 + 1)\hat{G}(\boldsymbol{\omega}) e^{2\pi i \mathbf{x}\cdot\boldsymbol{\omega}} \delta(\boldsymbol{\omega}-\boldsymbol{\omega}'). \tag{25}$$

Thus, integrating over $\boldsymbol{\omega}$ we obtain the Fourier transform of the Green's function for the $(\nabla^2 - 1)$ operator:

$$\hat{G}(\boldsymbol{\omega}) = -\frac{1}{4\pi^2|\boldsymbol{\omega}|^2 + 1}. \tag{26}$$

Now, we can approximate the integral in Eq. (20). Taking the leading order expansion of $1/(\delta_w k)$, we can re-write equation Eq. (20) as:

$$\begin{aligned} w(x) &= \int d\mathbf{x}\text{'} \int d\boldsymbol{\omega} \frac{1}{4\pi^2|\boldsymbol{\omega}|^2 + 1} e^{2\pi i \mathbf{x}\cdot\boldsymbol{\omega}} e^{-2\pi i \mathbf{x}\text{'}\cdot\boldsymbol{\omega}} (p/\nu + \phi_1 b), \\ &= \frac{p}{\nu} \int d\mathbf{x}\text{'} \int d\boldsymbol{\omega} \frac{1}{4\pi^2|\boldsymbol{\omega}|^2 + 1} e^{2\pi i \mathbf{x}\cdot\boldsymbol{\omega}} e^{-2\pi i \mathbf{x}\text{'}\cdot\boldsymbol{\omega}} \\ &+ \phi_1 \int d\mathbf{x}\text{'} \int d\boldsymbol{\omega} \frac{1}{4\pi^2|\boldsymbol{\omega}|^2 + 1} e^{2\pi i \mathbf{x}\cdot\boldsymbol{\omega}} e^{-2\pi i \mathbf{x}\text{'}\cdot\boldsymbol{\omega}}\, b \end{aligned} \tag{27}$$

First, we solve the integral in Eq. (27) which does not depend on b:

$$\frac{p}{\nu}\int d\mathbf{x'}\int d\boldsymbol{\omega}\frac{1}{4\pi^2|\boldsymbol{\omega}|^2+1}e^{2\pi i\mathbf{x}\cdot\boldsymbol{\omega}}e^{-2\pi i\mathbf{x'}\cdot\boldsymbol{\omega}}, \tag{28a}$$

$$=\frac{p}{\nu}\int d\boldsymbol{\omega}\frac{1}{4\pi^2|\boldsymbol{\omega}|^2+1}e^{2\pi i\mathbf{x}\cdot\boldsymbol{\omega}}\delta(\boldsymbol{\omega}), \tag{28b}$$

$$=\frac{p}{\nu}. \tag{28c}$$

To go from Eq (28a) to Eq. (28b) we integrated $e^{-2\pi i\mathbf{x'}\cdot\boldsymbol{\omega}}$ over $\mathbf{x}'$, obtaining a delta function in $\boldsymbol{\omega}$, and because delta functions satisfy $\int d\mathbf{x}f(\mathbf{x})\delta(\mathbf{x})=f(\mathbf{0})$, Eq. (28c) follows. Now, following analogous steps, we integrate the part of Eq. (27) which depends on b. Letting $\hat{b}(\mathbf{x})$ be the Fourier transform of $b(x)$ we obtain:

$$\begin{aligned}
&\phi_1\int d\mathbf{x}'\int d\boldsymbol{\omega}\frac{1}{4\pi^2|\boldsymbol{\omega}|^2+1}e^{2\pi i\mathbf{x}\cdot\boldsymbol{\omega}}e^{-2\pi i\mathbf{x}'\cdot\boldsymbol{\omega}}b(\mathbf{x}')\\
&=\phi_1\int d\mathbf{x}'\int d\boldsymbol{\omega}\int d\boldsymbol{\omega'}\frac{1}{4\pi^2|\boldsymbol{\omega}|^2+1}e^{2\pi i\mathbf{x}\cdot\boldsymbol{\omega}}e^{-2\pi i\mathbf{x}'\cdot\boldsymbol{\omega}}e^{2\pi i\mathbf{x}\cdot\boldsymbol{\omega'}}\hat{b}(\boldsymbol{\omega'}),\\
&=\phi_1\int d\boldsymbol{\omega}\int d\boldsymbol{\omega'}\frac{1}{4\pi^2|\boldsymbol{\omega}|^2+1}e^{2\pi i\mathbf{x}\cdot\boldsymbol{\omega}}\hat{b}(\boldsymbol{\omega'})\int d\mathbf{x}'e^{-2\pi i\mathbf{x}\cdot(\boldsymbol{\omega}-\boldsymbol{\omega'})},\\
&=\phi_1\int d\boldsymbol{\omega}\int d\boldsymbol{\omega'}\frac{1}{4\pi^2|\boldsymbol{\omega}|^2+1}e^{2\pi i\mathbf{x}\cdot\boldsymbol{\omega}}\hat{b}(\boldsymbol{\omega'})\delta(\boldsymbol{\omega}-\boldsymbol{\omega'}),\\
&=\phi_1\int d\boldsymbol{\omega}\frac{1}{4\pi^2|\boldsymbol{\omega}|^2+1}e^{2\pi i\mathbf{x}\cdot\boldsymbol{\omega}}\hat{b}(\boldsymbol{\omega}),\\
&\simeq\phi_1\int d\boldsymbol{\omega}(1-4\pi^2|\boldsymbol{\omega}|^2+16\pi^4|\boldsymbol{\omega}|^4)e^{2\pi i\mathbf{x}\cdot\boldsymbol{\omega}}\hat{b}(\boldsymbol{\omega}),\\
&=\phi_1[b+\nabla^2 b+\nabla^4 b].
\end{aligned}$$

In the second to last line we expanded $1/(4\pi^2|\boldsymbol{\omega}|^2+1)$ around zero. This expansion can be justified by considering the smoothness of b: we do not expect vegetation to have any shock fronts, implying that b should be a smooth function. Therefore, its Fourier transform $\hat{b}(\boldsymbol{\omega})$ should decay quickly as $|\boldsymbol{\omega}|\to\infty$, meaning $\hat{b}(\boldsymbol{\omega})$ is peaked near at $\boldsymbol{\omega}=0$. In the last line of the derivation we used the Fourier identity,

$$(\nabla^2)^n b(\mathbf{x})=\int d\boldsymbol{\omega}(-4\pi^2|\boldsymbol{\omega}|^2)^n\hat{b}(\boldsymbol{\omega})e^{2\pi i\mathbf{x}\cdot\boldsymbol{\omega}}. \tag{29}$$

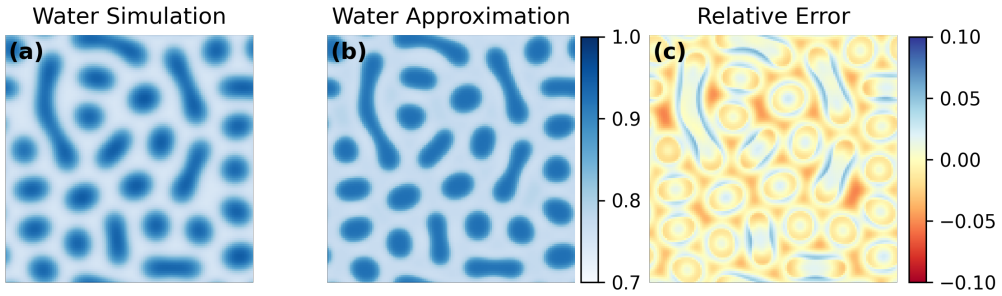

Figure 10: **(a)** The water field, w, resulting from simulating Eqs. (15). **(b)** The approximation $w = \frac{p}{\nu} + \phi_1[b + \nabla^2 b + \nabla^4 b] + \phi_2[b^2 + \nabla^2(b^2) + \nabla^4(b^2)]$ obtained by numerically fitting the parameters ϕ_i's to the simulated w in (**a**), using the corresponding biomass field, b from the simulation. **(c)** The relative error is within 5% for $\phi_1 \simeq -0.2$, and $\phi_2 \simeq -0.1$. The fitting of parameters was done using least squares.

Substituting these two results into Eq.(27) we obtain an equation for groundwater in terms of biomass and its spatial derivatives:

$$w(x) = \frac{p}{\nu} + \phi_1[b + \nabla^2 b + \nabla^4 b]. \tag{30}$$

We can do an analogous derivation, including higher powers of b in the expansion of $1/k^2$ in equation Eq. 27, to obtain a general equation for groundwater in terms of biomass of the form:

$$w(\mathbf{x}) = \frac{p}{\nu} + \phi_1[b + \nabla^2 b + \nabla^4 b] + \phi_2[b^2 + \nabla^2(b^2) + \nabla^4(b^2)] + \cdots \tag{31}$$

To calculate an example of a w equation of the form of Eq. (31), we use resulting b and w fields from simulating Eqs. (15) to numerically find the parameters ϕ_1 and ϕ_2. The water simulation, the resulting approximation, and the relative error are plotted in Fig. 10. It can be observed that for the least square fit values of ϕ_1 and ϕ_2 the relative error of approximation of w given by Eq. (31) is within 5%. These results indicate that for appropriate choices of the parameters we can get quite accurate approximations for the w field using Eq. (31).

4 A Swift-Hohenberg style model for vegetation patterns

The Swift-Hohenberg model was originally derived as an equation to describe the temperature and fluid velocity dynamics in thermal convection [14]. This equation has been interpreted as a model system for pattern formation, and therefore has been extensively studied in the last decades [10]. Previous studies have expanded the SH model to include non-local terms, in an effort to develop a generic model to account for the spatiotemporal dynamics of spatially extended systems [19].

In this work we present a Swift-Hohenberg-style model that arises from vegetation pattern modeling. In contrast with the original SH equation given by Eq. (10), our model includes non-linear terms multiplying the spatial derivatives of the equation, which is a reflection of the dynamics of our particular system.

The general form of our vegetation pattern formation model can be obtained by substituting the general form obtained for the groundwater, Eq. (31), into the biomass equation given in Zelnik's original model Eq. (15a), giving an equation for the biomass of the form:

$$\partial_t b = f(b) + g(b)\nabla^2 b + bh(b)\nabla^4 b, \tag{32}$$

where $f(b)$, $g(b)$ and $h(b)$ are polynomial functions in b.

To study the pattern formation properties of Eq. (32) we choose a simple form of Eq. (32) that conserves the water-vegetation dynamics of the system:

$$\partial_t b = f(b) + \epsilon(D_1 - b)\nabla^2 b - \epsilon^2 D_2 b\nabla^4 b, \tag{33}$$

where the ϵ terms come from the scaling of variables, $\tilde{x} = x/k$ we did to derive the $w(b)$ equation, and D_1 and D_2 are constants that depend on the form we choose for $w(b)$.

We know that $f(b) = \lambda b(1-b)(1+\eta b)^2 w_1(b)$, where $w_1(b)$ is the part of $w(b)$ which do not depends on gradients of b. As suggested by the leading order coefficients of the initial ϵ^2/k^2 expansion given by the right hand side of equation (19), in combination with comparison to our numerical simulations, we choose

$$w_1(b) = \frac{p}{\nu}(1 - b(p\nu - \lambda)). \tag{34}$$

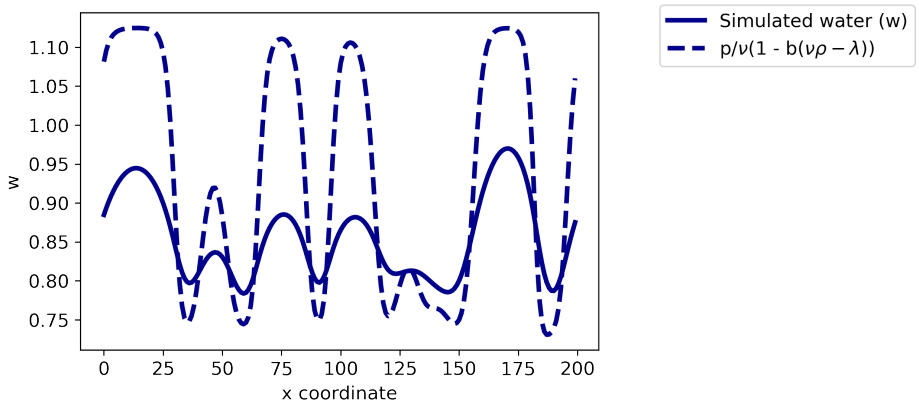

Figure 11: Water (solid line) resulting from simulating Eqs. (15), and water approximation (dashed line) given by Eq. (34). Notice that even though we are taking a linear approximation in the biomass, it already captures the general shape of the simulated water field. This line plot is a cross section of the labyrinths patterns presented in Fig. 9 after 30 years of simulation

It can be observed in Fig. 11 that this approximation successfully captures the general shape of the simulated water field. Moreover, the feedback mechanism of soil-water diffusion, which dominates in the system studied suggests that the spatial distribution of water should mirror that of biomass: areas of denser vegetation will have low groundwater and vice-versa. Thus, to leading order, it is reasonable to assume that $w(b) = \gamma_0 - b\gamma_1$, where γ_i is constant for $i = 0, 1$.
Hence, we explore an equation for biomass of the form:

$$b_t = \frac{p\lambda}{\nu} b(1-b)(1+\eta b)^2(1-b(\rho\nu-\lambda)) + \epsilon(D_1 - b)\nabla^2 b - \epsilon^2 D_2 b \nabla^4 b. \quad (35)$$

where $\epsilon \sim \frac{1}{k^2} \sim \delta_w \sim 100$, and $D_1 = D_2 = 0.1$. To study the pattern formation characteristics of this equation we perform a linear stability analysis of the system. To find homogeneous steady states we solve:

$$0 = \frac{p\lambda}{\nu} b(1-b)(1+\eta b)^2(1-b(\rho\nu-\lambda)). \quad (36)$$

The steady states as a function of precipitation P can be observed in Fig. 12. Similarly to the 2 equations model, we observe bi-stability of steady states,

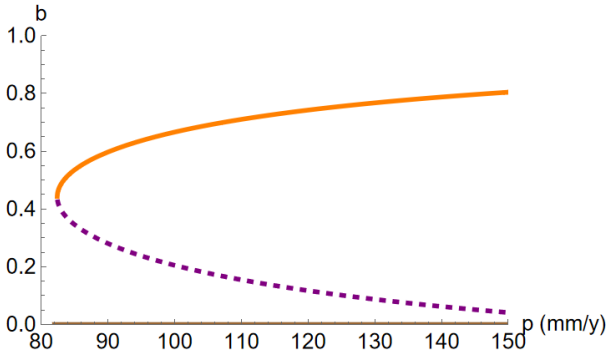

Figure 12: Bifurcation diagram of the steady states of the reduced biomass model, showing the non-dimensional biomass (b) vs. the precipitation rate in dimensions of mm/y. The full (dashed) lines correspond to stable (unstable) equilibria. Similarly to the original two-equation model we observe the bi-stability of stable states.

which indicates the existence of spatially patterned states as different regions approach different stable equilibria as set by their local initial conditions.

We now study the growth of a perturbation of the uniformly stable steady state $u_\star$. We consider a small perturbation of the form $b_p = Ae^{\sigma t + i\mathbf{x}\cdot\mathbf{q}}$, and study how the growth rate, σ depends on the precipitation P and the wave number $\mathbf{q}$. The perturbation b_p evolves according to the equation

$$\partial_t b_p = N[b_\star - b_p] - N[b_\star], \tag{37}$$

where N is defined as

$$N[b] = \frac{p\lambda}{\nu} b(1-b)(1+\eta b)^2(1-b(\rho\nu-\lambda)) - b + \epsilon(D_1 - b)\nabla^2 b - \epsilon^2 D_2 \nabla^4 b. \tag{38}$$

Letting

$$f(b) = \frac{p\lambda}{\nu} b(1-b)(1+\eta b)^2(1-b(\rho\nu-\lambda)), \tag{39}$$

we find that the perturbation b_p follows the evolution equation:

$$\partial_t b_p = \left(\left.\frac{\partial f}{\partial b}\right|_{b_\star} + \epsilon(D_1 - b_\star)\nabla^2 - \nabla^2 b_\star - \epsilon^2 D_2 b_\star \nabla^4 - \epsilon^2 D_2 \nabla^4 b_\star \right) b_p, \quad (40a)$$

$$= \left(\left.\frac{\partial f}{\partial b}\right|_{b_\star} + \epsilon(D_1 - b_\star)\nabla^2 - \epsilon^2 D_2 b_\star \nabla^4 \right) b_p, \quad (40b)$$

where one may proceed from Eq. (40a) to Eq. (40b) by noticing the gradients of $b_\star$ vanish because we assumed $b_\star$ to be an homogeneous steady state. Substituting $b_p = Ae^{\sigma t + i\mathbf{x}\cdot\mathbf{q}}$ into the equation above, we obtain an equation for the growth rate of a mode with wave number q:

$$\sigma_q = \left.\frac{\partial f}{\partial b}\right|_{b_\star} - \epsilon(D_1 - b_\star)q^2 - \epsilon^2 D_2 b_\star q^2 \quad (41)$$

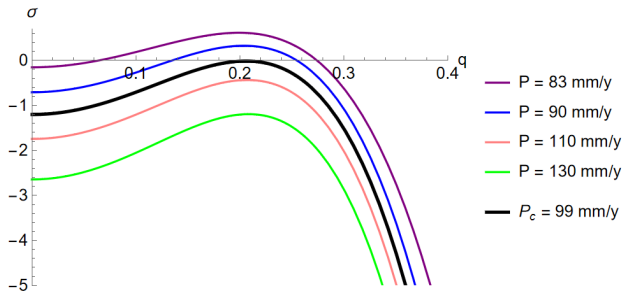

Figure 13: Growth rate σ_q vs. the wave number q for the non-zero uniform stable state of equation (15a) for different values of the precipitation parameter P. The marginally stable state (black line) occurs at $P_c \simeq 99$: below this precipitation value, instabilities will grow, creating patterns with characteristic wavelength $q_c \sim 0.2$.

Fig. 13 shows the growth rate σ versus the wave number q for different values of the precipitation parameter P. This plot reveals that the uniform steady state $b_\star$ becomes unstable in the presence of diffusion for precipitation values below $P_c = 99$. The maximum growth rate occurs at a finite wavelength, indicating the presence of a non-uniform instability. Therefore, we expect Eq. (35) to give rise to patterned states.

Our simulation results are shown in Fig. 14, where the variety of patterned states that emerge from Eq. (35) are apparent. It is also important to notice that the characteristic length scale of the patterns is comparable to that of the original model, which indicates that our equation satisfactorily describes the emergent vegetation patterns.

The equation derived in this paper, Eq. (35), differs from the original SH model given by Eq. (10) in that it includes polynomial functions of b multiplying its spatial derivatives. In the context of vegetation, these terms reflect that biomass regulates its own water dependent biomass growth. If more water is added through the system, biomass will selectively grow in the places where vegetation is already denser. Moreover, although biomass consumes water, it also reduces its evaporation. These intricate water-biomass dynamics differentiate vegetation patterning from classical activator-inhibitor systems and therefore we obtain a modified SH model where biomass regulates its own diffusion and higher order spatial derivatives.

5 Conclusions

The present work has introduced a Swift-Hohenberg style model to describe pattern formation of dryland vegetation. Our model consists of a single equation describing the evolution of biomass. It has the novelty of introducing polynomial functions of biomass multiplying spatial second and fourth derivatives, which takes into account the water-vegetation dynamics of the system studied. By performing a linear stability analysis of our new, one equation model, we find the coexistence of two stable states under a wide range of precipitation values. This bi-stability constitutes a meaningful property of systems that exhibit pattern formation and it is also present for the original Zelnik *et al.* [9] model. The linear stability analysis also reveals a range of precipitation values for which perturbations around the uniform vegetation stable state of the system will grow. This instability occurs at non-zero wave number, indicating the appearance of spatially periodic patterns. Moreover, the wave lengths of these unstable modes, which dictate the scale of the pattern formed, are consistent with the length scales observed for vegetation patterns.

We performed numerical simulations of this new model and observed a wide range of patterns, including spots, hexagonal patterns and labyrinths. These initial results suggest that our reduced model successfully captures the

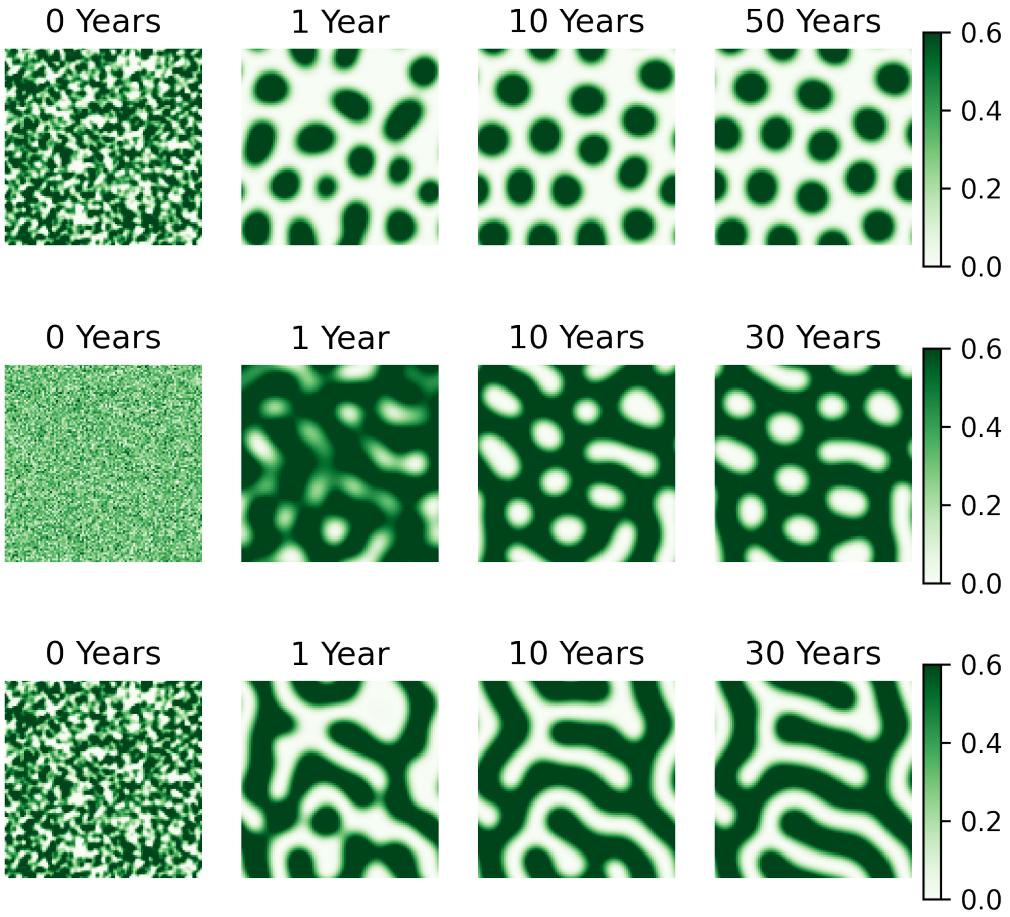

Figure 14: Patterns resulting from modeling Eq. (35). The first was simulated with a precipitation value of $P = 90$, while the second and third rows were simulated with a precipitation value $P = 100$. All of our simulations were started from random noise. The second row reveals a labyrinth pattern, while the first and third rows show hexagonal patterns of vegetation spots and gaps respectively. Dark green indicates vegetation and white corresponds to bare soil.

dynamics of the evolution of biomass in a water limited ecosystem. Given the form of equation 15a, our model is easily mathematically tractable, and can be used to study drivers of ecosystem collapse. This work showed that for precipitation values below $90mm/y$ an uniform vegetation cover becomes

unstable, thus in the absence of pattern formation these conditions would drive the system to desertification. We suggest further work to study the stability of the different periodic patterns to gain a better understanding of the conditions under which the system would not be able to sustain any vegetation. Moreover, given the clear ecological meaning of the coefficients in our model, one can study the dynamics of the system under different values of the ecological factors. For instance, by considering how the dynamics of the system change when we vary evaporation, we could account for the current changes in temperatures of ecosystems.

Moreover, we propose a generalization, Eq. (35) of the original Swift-Hohenberg model to include polynomial functions multiplying spatial derivatives terms. In this work we showed an application of this model to ecology, however the richness of Eq. (35) suggests that it might be able to describe the dynamics of other physical and biological systems. Previous work has suggested other generalizations of the SH model, such as the the inclusion of non-local nonlinearities [20]. Therefore, the dynamics of more general SH style models such as the one we propose in this work appears as an interesting area of study.

6 Acknowledgments

I'd like to thank Alasdair Hastewell and Davis Evans for mentoring this project. I'd also like to thank Prof. John Bush, Prof. Jörn Dunkel, and Dr. Ousmane Kodio for suggesting this project and for their insights and suggestions throughout the summer. I'd also like to thank Slava Gerovitch, Barbara Peskin, Prof. Ankur Moitra, and Prof. David Jerison for organizing MIT's Summer Program in Undergraduate Research (SPUR), where this research was conducted.

References

[1] D. Etling and R. A. Brown. Roll vortices in the planetary boundary layer: A review. *Boundary-Layer Meteorology*, 65:215–248, 1993.

[2] Martin J. How and Johannes M. Zanker. Motion camouflage induced by zebra stripes. *Zoology*, 117(3):163–170, 2014.

[3] Paolo D'OdoricoAmilcare PorporatoChristiane Wilkinson Runyan. *Dryland Ecology*. Springer, Cham, 2019.

[4] Meron Ehud. Vegetation pattern formation: The mechanisms behind the forms. *Physics Today*, 72(11):30–36, 2019.

[5] Paolo D'Odorico, Abinash Bhattachan, Kyle F. Davis, Sujith Ravi, and Christiane W. Runyan. Global desertification: Drivers and feedbacks. *Advances in Water Resources*, 51:326–344, 2013. 35th Year Anniversary Issue.

[6] Nadir Jeevanjee and David M. Romps. Mean precipitation change from a deepening troposphere. *Proceedings of the National Academy of Sciences*, 115(45):11465–11470, 2018.

[7] Easton White and Alan Hastings. Seasonality in ecology: Progress and prospects in theory. 09 2018.

[8] J. von Hardenberg, E. Meron, M. Shachak, and Y. Zarmi. Diversity of vegetation patterns and desertification. *Phys. Rev. Lett.*, 87:198101, Oct 2001.

[9] Yuval R. Zelnik, Ehud Meron, and Golan Bel. Gradual regime shifts in fairy circles. *Proceedings of the National Academy of Sciences*, 112(40):12327–12331, 2015.

[10] M. C. Cross and P. C. Hohenberg. Pattern formation outside of equilibrium. *Rev. Mod. Phys.*, 65:851–1112, Jul 1993.

[11] Turing Alan Mathison. The chemical basis of morphogenesis. *Phil. Trans. R. Soc. Lond.*, 237:37–72, 1952.

[12] Michael Cross and Henry Greenside. *Pattern Formation and Dynamics in Nonequilibrium Systems*. Cambridge University Press, 2009.

[13] Nonlinear Physics of Ecosystems. *Ehud Meron*. CRC Press, 1 edition, 2015.

[14] J. Swift and P. C. Hohenberg. Hydrodynamic fluctuations at the convective instability. *Phys. Rev. A*, 15:319–328, Jan 1977.

[15] E. Gilad, J. von Hardenberg, A. Provenzale, M. Shachak, and E. Meron. Ecosystem engineers: From pattern formation to habitat creation. *Phys. Rev. Lett.*, 93:098105, Aug 2004.

[16] *Nonlinear Dynamics and Chaos: With Applications to Physics, Biology, Chemistry, and Engineering (2nd ed.).*

[17] Escaff D. Fernandez-Oto C., Tlidi M. and Clerc M. G. Strong interaction between plants induces circular barren patches: fairy circles. *Phil. Trans. R. Soc.*, 2014.

[18] Jonathan A. Sherratt. An analysis of vegetation stripe formation in semi-arid landscapes. *Journal of Mathematical Biology*, 2005.

[19] Axel Hutt. Generalization of the reaction-diffusion, swift-hohenberg, and kuramoto-sivashinsky equations and effects of finite propagation speeds. *Phys. Rev. E*, 75:026214, Feb 2007.

[20] David Morgan and Jonathan H.P. Dawes. The swift–hohenberg equation with a nonlocal nonlinearity. *Physica D: Nonlinear Phenomena*, 270:60–80, 2014.